THE JOURNAL OF PHYSICAL CHEMISTRY C

Article

pubs.acs.org/JPCC

Utilizing Wide Band Gap, High Dielectric Constant Nanoparticles as Additives in Organic Solar Cells

Ryan S. Gebhardt,[†,‡] Pengfei Du,[§] Akshit Peer,[‡] Mitch Rock,[∥] Michael R. Kessler,[∥] Rana Biswas,[‡,⊥,#] Baskar Ganapathysubramanian,[§] and Sumit Chaudhary*[,†,‡]

[†]Department of Materials Science and Engineering, [‡]Department of Electrical and Computer Engineering, [§]Department of Mechanical Engineering, and [⊥]Department of Physics and Astronomy, Iowa State University, Ames, Iowa, United States

[∥]School of Mechanical and Materials Engineering, Washington State University, Pullman, Washington, United States

[#]Ames Laboratory of the U.S. DOE, Ames, Iowa, United States

Supporting Information

ABSTRACT: We experimentally and theoretically investigate the effects of utilizing $BaTiO_3$ nanoparticles as additives in polythiophene/fullerene solar cells. $BaTiO_3$ nanoparticles were chosen because of their multifaceted potential for increasing exciton dissociation (due to their high dielectric constant) and light scattering. To achieve stable suspensions for device fabrication, the nanoparticles were functionalized with organic ligands. Solar cells fabricated in air showed ∼40% enhancement in the photocurrent primarily due to string-like aggregates of functionalized $BaTiO_3$ particles that increase light absorption without hindering charge collection. Solar cells fabricated in an inert atmosphere yielded overall more efficient devices, but the string-like aggregates were absent and enhancement in photocurrent was up to ∼6%. Simulations with the excitonic drift-diffusion model demonstrate that a bare nanoparticle significantly increases exciton dissociation, whereas the functional group negates this effect. Simulations utilizing the scattering matrix method reveal that absorption enhancements caused by light scattering increase as the nanoparticles aggregate into string-like structures. These results offer insights for morphological design of ternary-blend bulk-heterojunction organic solar cells.

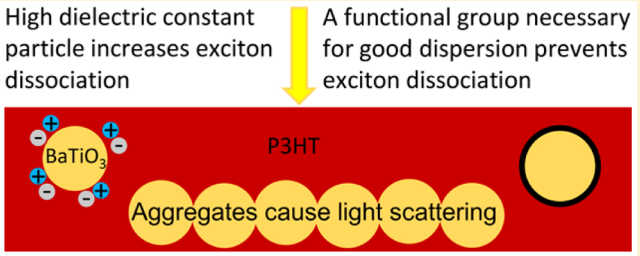

1. INTRODUCTION

Organic photovoltaics (OPVs) have received much attention in recent years as a possible renewable energy source and have recently achieved power conversion efficiencies more than 10%.[1] Their low cost, flexibility, and ease of fabrication make them an attractive alternative to other photovoltaic options. However, OPVs still have many loss mechanisms that need to be addressed in order to be cost competitive with other technologies. These loss mechanisms include incomplete absorption, thermalization loss, and exciton and free carrier recombination.[2] Many ternary blends have been investigated with typical bulk heterojunction (BHJ) materials such as poly-3-hexyl thiophene (P3HT) and phenyl-C_{61}-butyric acid methyl ester (PCBM) in order to address one or more of these losses. For instance, all organic blends have been used to enhance absorption in the typical P3HT:PCBM BHJ by adding a squaraine dye and utilizing Förster resonance energy transfer.[3] Another example of an all-organic ternary blend was the inclusion of high density polyethylene in P3HT:PCBM to facilitate easier fabrication processes and improve mechanical properties.[4] In yet another all-organic ternary system, ferroelectric PVDF-TrFE was added to P3HT:PCBM in order to increase exciton dissociation.[5,6]

Many attempts, though not always successful, have been made to add metallic nanoparticles (NPs) to the active-layer in order to increase absorption through light scattering and plasmonic enhancements.[7,8] While the absorption and even mobility[9] were increased in some cases, the overall performance was not always enhanced due to increased carrier recombination at the polymer−NP interface.

Ternary blends with semiconducting quantum dots have also been fabricated.[10−12] These quantum dots typically absorb light complementary to the absorption of the organic hosts, allowing absorption of a larger fraction of the solar spectrum, and leading to a possibility of higher output currents. Quantum dots can also be used to sensitize the BHJ to a specific wavelength for photodetector applications. However, these quantum dots are typically capped with insulating organic ligands, which can hinder charge transport and make electronic coupling with the host conjugated-organic matrix challenging.[13]

Inorganic oxide NPs have also been investigated as additives in BHJs. Cr_2O_3 NPs added to P3HT:PCBM OPVs led to higher efficiency, which was attributed to a better polymer

Received: September 2, 2015
Revised: October 1, 2015
Published: October 2, 2015

DOI: 10.1021/acs.jpcc.5b08581
J. Phys. Chem. C 2015, 119, 23883−23889

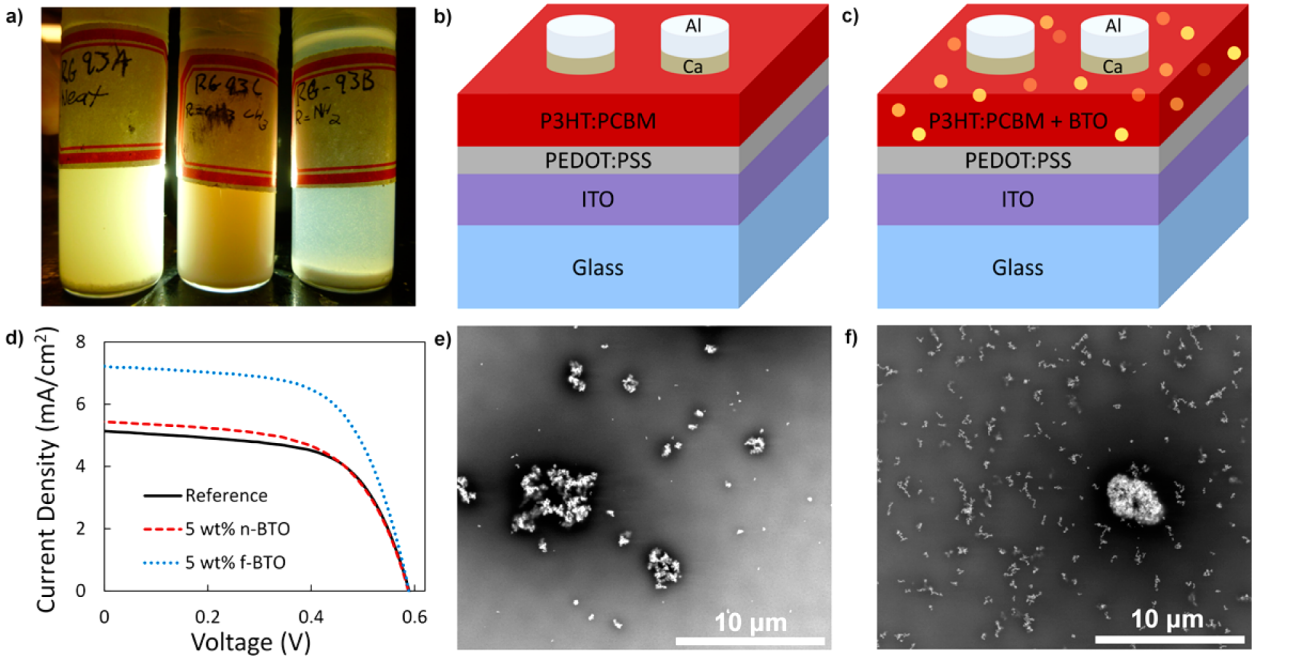

Figure 1. (a) From left to right: neat, methyl-, and amine-functionalized BTO particles in DCB several minutes after sonicating. Schematic of the solar cell device structure (b) without and (c) with BTO particles. (d) Photocurrent density vs voltage curves for a reference device and devices made with neat (n-BTO) and functionalized (f-BTO) particles. Backscattered electron SEM image for (e) n-BTO and (f) f-BTO particles, which shows string-like aggregates, in P3HT:PCBM.

morphology, increased absorption, enhanced electron mobility and reduced hole leakage current.[14] In another study, barium titanate (BTO) NPs were added in a very low concentration to P3HT:PCBM in order to increase mechanical robustness of flexible solar cells.[15] The hard ceramic particles prevented the metal contacts from shorting together during bending and lamination. Though the fill factor (FF) and short-circuit current (J_{sc}) reduced slightly with the BTO addition, the open circuit voltage increased slightly, and thus, the overall efficiency was more or less the same. The authors concluded that the low concentration of BTO did not significantly affect the optoelectronic properties of the device. However, a similar experiment with ZnO NPs drastically reduced the solar cell performance.[15] This was attributed to the undesirable conduction band energy level of ZnO that could cause electrons to be trapped on the NP.

In all of these ternary blends, the third phase may affect properties other than the intended purpose. For example, many of the plasmonic NPs increase absorption but can introduce trap states and increase recombination.[7−9] In many of these cases, the third additive material can act as a bottleneck for charge transport. Therefore, it is critical to understand and optimize the distribution of the ternary phase in BHJ blends. Herein we further study the effects of BTO on the optoelectronic properties of P3HT:PCBM solar cells. Coupling simulations and experiments, we investigate how adding a functional group and changing the NP distribution affect the OPV properties and performance.

2. MATERIALS AND METHODS

We chose BTO as an additive due to its high dielectric constant. It has been shown that increasing the dielectric constant of the absorbing layer can increase the exciton dissociation efficiency in a BHJ, which can be attributed to reduced exciton binding energy.[16] The equation describing the exciton dissociation rate (adapted from ref 16) is

$$D = \frac{3\gamma}{4\pi a^3} e^{-E_B/k_B T}\left(1 + b + \frac{b^2}{3} + \frac{b^3}{18} + \ldots\right)X \quad (1)$$

where a is the initial separation distance, E_B is the exciton binding energy, k_B is the Boltzmann constant, T is temperature, and X is the exciton concentration, and γ (Langevin recombination parameter) and b are

$$\gamma = \frac{q}{\varepsilon}\min(\mu_n, \mu_p) \quad (2)$$

$$b = \frac{q^3 E}{8\pi\varepsilon k_B^2 T^2} \quad (3)$$

where q is the electron charge, ε is the permittivity of the absorber, $\mu_{n/p}$ is the electron/hole mobility, and E is the electric field strength. While adding BTO is not expected to affect the exciton binding energy or permittivity in the polymer, it can alter the built-in electric field (E) of the device, thus potentially increasing exciton dissociation at the polymer−BTO interface and assisting charge transport.

3. RESULTS

At the outset, we attempted dispersing 50 nm BTO particles (U.S. Nano) in 1,2-*ortho*-dichlorobenzene (DCB), a popular solvent employed for dissolution of OPV active-layer materials. After adding the neat BTO particles to DCB and sonicating, the particles appeared well-dispersed, but within a few seconds, the particles began to aggregate and precipitate. In order to prevent aggregation of the BTO particles, they were functionalized with methyl- and amine-terminated coupling agents via a silanization process (see methods in SI). After sonicating with a probe sonicator, the methyl-functionalized particles stayed suspended

DOI: 10.1021/acs.jpcc.5b08581
J. Phys. Chem. C 2015, 119, 23883−23889

Table 1. Photovoltaic Properties of Three Exemplary Sets of Devices[a]

set	sample	J_{sc} (mA/cm^2)	fill factor	PCE (%)
1 (air)	reference	5.13 ± 0.17	62.1 ± 0.9	1.87 ± 0.08
	5 wt % neat BTO	5.47 ± 0.16	59.4 ± 0.5	2.00 ± 0.06
	5 wt % f-BTO	7.21 ± 0.33	62.9 ± 0.4	2.72 ± 0.14
2 (glovebox)	reference	9.43 ± 0.17	55.8 ± 2.6	3.24 ± 0.15
	2.5 wt % f-BTO	9.53 ± 0.18	53.7 ± 1.6	3.15 ± 0.13
	5 wt % f-BTO	9.23 ± 0.25	51.1 ± 2.0	2.90 ± 0.16
	10 wt % f-BTO	9.15 ± 0.19	49.2 ± 1.7	2.76 ± 0.08
3 (glovebox)	reference	9.30 ± 0.31	54.6 ± 1.7	3.08 ± 0.14
	2 wt % f-BTO	9.55 ± 0.25	55.9 ± 3.3	3.27 ± 0.24
	5 wt % f-BTO	9.88 ± 0.23	51.0 ± 2.2	3.07 ± 0.09
	10 wt % f-BTO	9.89 ± 0.28	51.7 ± 0.6	3.12 ± 0.05

[a]Reported standard deviations based on a sample size of 6.

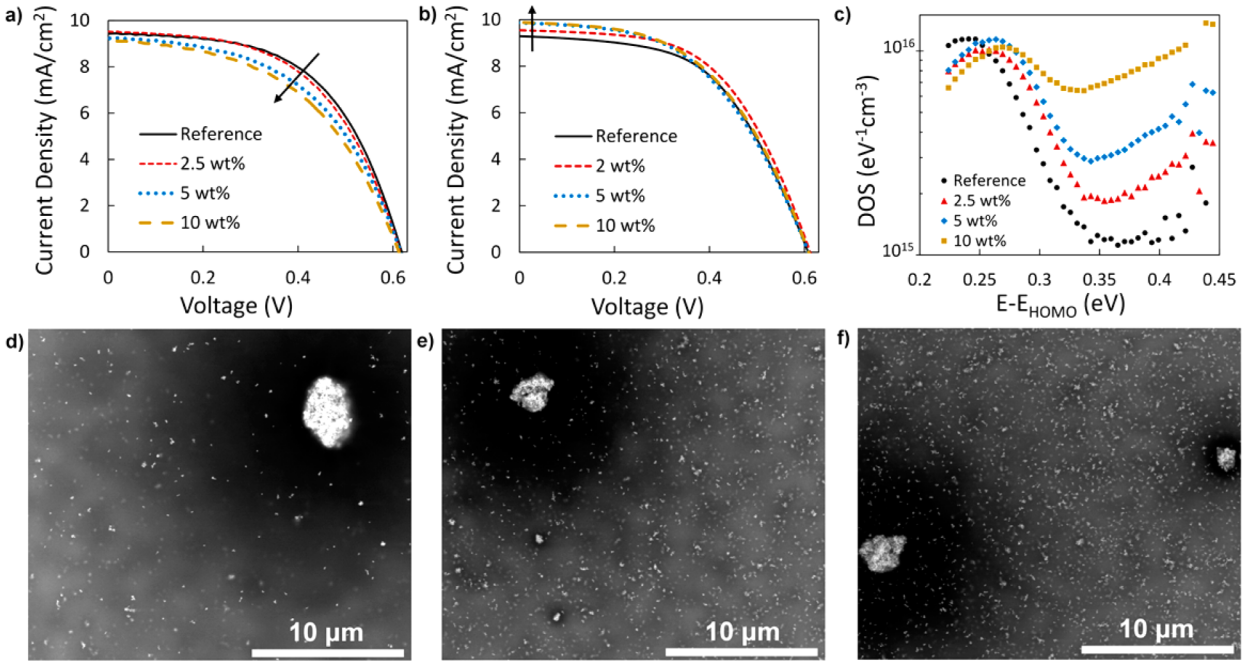

Figure 2. (a) Photocurrent density vs voltage curves for a set of devices showing a decrease in FF with f-BTO particle additions and (b) curves for similarly fabricated devices showing an increase in J_{sc}. (c) Density of trap states for devices containing 2.5, 5, and 10 wt % f-BTO. (d, e, and f) Backscattered electron SEM images for active-layers containing 2.5, 5, and 10 wt % f-BTO, respectively.

in DCB for more than 1 week before notable aggregation and precipitation, whereas the neat and amine-functionalized particles aggregated and began precipitating within a few minutes, as shown in Figure 1a.

As the methyl-functionalized BTO (f-BTO) particles showed the best dispersion, these particles were chosen to be added to the active-layer of P3HT:PCBM solar cells (structure shown in Figure 1b,c). To investigate the effect of the functional group on the composite film, P3HT:PCBM solar cells were fabricated with both neat BTO and f-BTO particles at five weight percent (wt %) additions. These devices were fabricated outside the glovebox so that the solutions could be sonicated immediately before use. The current−voltage (I−V) characteristics (Figure 1d, Table 1, set 1) showed a marginal increase (6%) in the J_{sc} for the sample with neat BTO particles and a larger increase (40%) with the f-BTO particles compared to a reference cell. Scanning electron microscope (SEM) images of active-layers of these samples are shown in Figure 1e,f. The sample with neat BTO particles showed mostly large aggregates and a poor distribution of the particles. Since a carrier generated on one side of an aggregate would have to travel a long distance around the aggregate to reach the electrode, these large aggregates certainly hinder charge collection. This may be the reason for the slightly reduced FF (59 vs 62 for the reference) of the sample with neat BTO particles. It is interesting that there is still some enhancement in J_{sc} for the neat BTO sample, which may be caused by enhanced exciton dissociation and collection near the small aggregates or even near the edges of the large aggregates. The sample with f-BTO particles showed a few large aggregates, but the distribution was much better with small, string-like aggregates, which are not as much of a hindrance to charge collection and offers larger enhancement.

Since the f-BTO particles stay dispersed for a long time, we continued our study by fabricating devices inside a glovebox, which yielded more efficient devices. Solutions with 40 mg/mL total P3HT:PCBM concentrations in DCB were used with additions of 2.5, 5, and 10 wt % of f-BTO particles. The device performance for similarly fabricated devices proved to be inconsistent. For one set, the J_{sc} of the samples with f-BTO particles was more or less similar to that of the reference, but

DOI: 10.1021/acs.jpcc.5b08581
J. Phys. Chem. C 2015, 119, 23883−23889

the FF suffered, leading to decreased power conversion efficiency (PCE; Table 1, set 2). In the other set, the J_{sc} increased with f-BTO and, except for the case of 2 wt %, the FF reduced (Table 1, set 3). This behavior led to similar or slightly enhanced PCE compared to the reference. Figure 2a,b shows the average $I-V$ curves for both of these sets. To further investigate what might be causing these differences between sets, we performed capacitance measurements to investigate the effect of f-BTO particle concentration on trap states, used SEM to examine the dispersion of f-BTO particles in the active-layer of the devices, and used simulations to study the relationship between the distribution of BTO particles and optoelectronic properties of devices.

We characterized capacitance as a function of frequency for samples with different f-BTO loadings. The equivalent circuit was properly chosen for different frequency regimes (series model at high frequency and parallel-model at lower frequency) and the density of trap states was calculated using methods reported elsewhere.[17,18] The addition of the f-BTO particles clearly increases the density of trap states as shown in Figure 2c. The trap states likely stem from a disruption in the electronic environment at the interface of the functional group and P3HT:PCBM. The extra trap states can lead to increased recombination and hinder charge collection, which can partially be the reason behind reduced FF in f-BTO devices.

Figure 2d–f shows the SEM images of P3HT:PCBM active-layers with different loadings of f-BTO particles. We observed some large aggregates in all samples and a different microstructure than the samples fabricated in air. The f-BTO particles in this set were better dispersed and did not show string-like aggregation that the samples fabricated in air showed (Figure 1f). As the loading increased from 2.5 to 10 wt %, the amount of small aggregates increased, however, the string-like aggregates observed in the air-fabricated sample were absent. We hypothesized that stirring, due to its directional motion, might cause anisotropic aggregates to form. While stirring for longer times did increase the amount of aggregates (Figure S1), we were unable to replicate the string-like aggregates, which showed the largest enhancement.

4. EXCITONIC DRIFT-DIFFUSION MODEL

To further understand the impact of a high dielectric constant nanoparticle on the optoelectronic properties, we performed simulations using the excitonic drift-diffusion model[19−21] (see methods in SI). While this simulation neglects the effect of trap states, it provides insight into the electric field distribution, exciton dissociation, and current densities in the active-layer. To simplify the simulations, we used a P3HT:PCBM bilayer and placed the particle in the P3HT domain since very few excitons are generated in the PCBM. The dimensions are chosen (shown in Figure 3a) so that the 50 nm particle takes up ∼3% of the total volume. This is in good agreement with experiment since f-BTO additions of 2.5, 5, and 10 wt % lead to ∼1.1, 2.1, and 4.2% f-BTO by volume (vol %) due to the difference in densities of P3HT (1.1 g/cm^3), PCBM (1.5 g/cm^3), and BTO (6.02 g/cm^3). The reported dielectric constant of nanocrystalline BTO varies widely (∼80−1000) depending on the crystal size and the synthesis and measuring techniques.[22−27] Our initial simulation of a particle with a relatively conservative dielectric constant of 150 showed a large enhancement in J_{sc} (6.3 compared to 3.6 mA/cm^2 for the reference). This increase in current (Figure 3b–d) is primarily attributed to increased exciton dissociation at the particle–

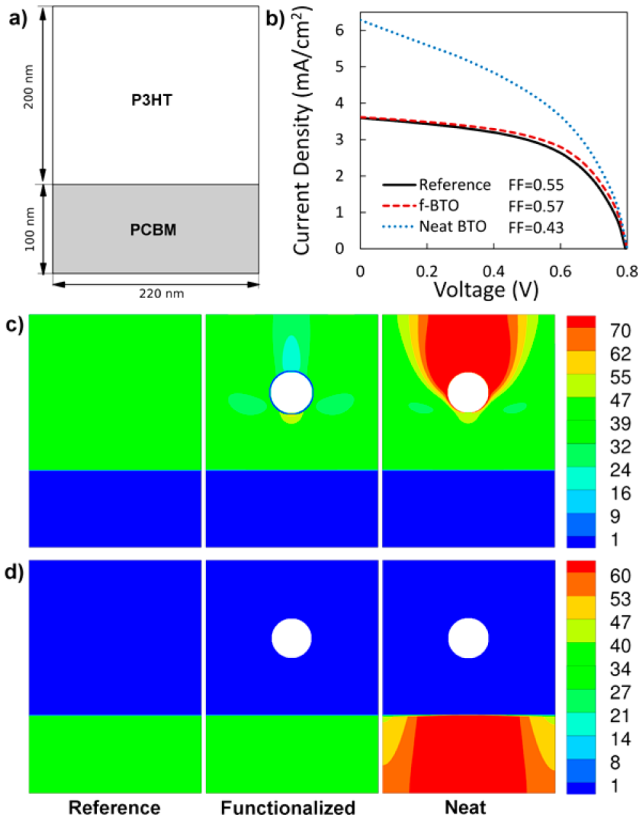

Figure 3. (a) Chosen geometry for the simulation. (b) Simulated photocurrent density vs voltage curves for a reference device, functionalized particle, and neat particle. (c, d) Hole and electron current density (A/m^2) contour plots at short circuit, respectively; left, reference; middle, functionalized particle; right, neat particle.

polymer interface (Figure S2). This simulation, however, was for a neat NP with no functional group. To more accurately simulate the functionalized particles used in our experiments, simulations were done with an insulating, low dielectric constant layer of 3 nm thickness added to the particle. This layer proved to negate the benefit of extra exciton dissociation completely as shown in Figure S2. The simulation still showed a very slight enhancement in PCE due to the electric field strength being higher in the active-layer (Figure S3), which assisted charge transport. While the neat NP shows a large increase in J_{sc}, it has a significantly reduced FF. The reasons are 2-fold: (1) As the cell voltage increases, the induced electric field around the particle decreases. For the case with the neat NP, the weaker electric field diminishes the dissociation effect of the high dielectric constant particle. (2) With a weaker electric field, the charges generated around the particle cannot be transported efficiently, which also results in higher recombination due to increased local charge density. Because the enhancement in exciton dissociation and charge collection are reduced with forward bias, so is the current enhancement.

5. OPTICAL EFFECTS

Learning that the functional group necessary to achieve a reasonable dispersion largely negates the enhancement in exciton dissociation, we investigated if the f-BTO particles can increase photocurrent due to enhancement in optical absorption. As BTO has a wide band gap and does not absorb visible light, it is expected that less light will be absorbed in the active-layer unless the particles cause significant scattering due

DOI: 10.1021/acs.jpcc.5b08581
J. Phys. Chem. C 2015, 119, 23883−23889

to the refractive index contrast between the organic material and the particles. Since the particles are small compared to the wavelength of visible light, the scattering is expected to be small. However, as the particles begin to aggregate so that their extent in at least one dimension approaches visible wavelengths, the scattering should increase. By comparing the global and specular transmissions, we can evaluate if light scattering is occurring. As any scattered light should be captured in the global measurement, we expect the global transmission to be higher than the specular transmission if any scattering is occurring. As shown in Figure 4, the global and specular transmissions are similar for the reference and 2.5 wt % f-BTO samples. The sample with 5 wt % shows a very small increase in global transmission compared to specular and the sample with 10 wt % shows a larger increase. As these samples showed more aggregation, we expect scattering to be more. The samples with f-BTO particles also showed slightly lower overall transmission compared to the reference. We found that the thickness (measured via SEM cross sections) of the active-layer increased from 213 ± 6.7 nm for the reference device to 256 ± 19.8, 273 ± 21.5, and 274 ± 32.8 nm for 2.5, 5, and 10 wt % f-BTO particle additions, which reduces the total transmission. To get a better sense of how the NP distribution affects absorption, we performed optical simulations using the rigorous scattering matrix (SM) method.[28,29]

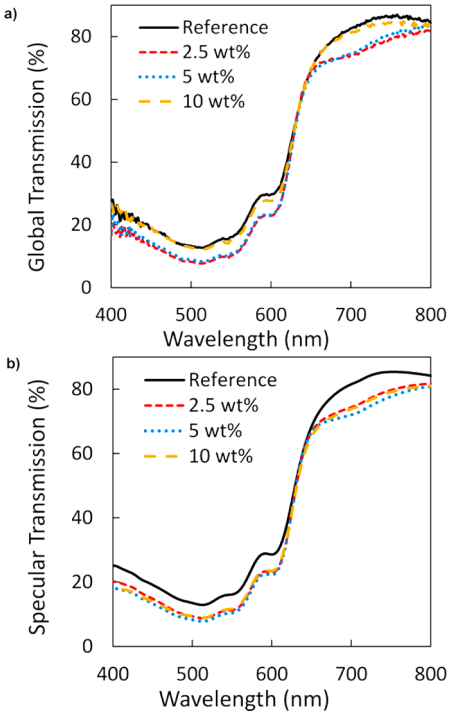

Figure 4. Measured (a) global and (b) specular transmission curves for a P3HT:PCBM reference device and devices with 2.5, 5, and 10 wt % f-BTO particles.

6. OPTICAL MODELING

As the SEM images for the best performing f-BTO based devices show strings of NPs within the active-layer, we adopted cuboids of dielectric material to model the NP aggregates. These NP strings were employed in the square lattice for computational ease, which allowed us to calculate the filling fraction of the NP strings relative to the organic material. We simulated single NP strings as well as multiple strings in a 300 nm thick active-layer of the solar cell. The former provided a lower loading (<2 vol %) as compared to the latter. The position of the NP strings in the z-direction was optimized for a single string to maximize the enhancement, as shown in Figure 5a. For a lattice pitch (a) of 300 nm and NP string width (w) and length ($l < a$) of ∼50 and ∼250 nm, respectively, the maximum enhancement was obtained when string is $z_2 \sim 170$ nm away from the organic-metal interface (Figure 5b). This is consistent with the standing wave formation theory, which suggests that the string should be either $\lambda/4n_{org}$ or $3\lambda/4n_{org}$ away from the organic−metal interface, where the electric field intensity is the largest.[30] By taking into account the width of the NP string and penetration of the field inside the metal (∼20 nm), this distance is ∼170 nm, corresponding to three-quarters of the wavelength inside the organic material ($3\lambda/4n_{org}$). It is to be noted that there is another weak maxima at $z_2 \sim 40$ nm that corresponds to the expected quarter wavelength in organic material ($\lambda/4n_{org}$), but this positioning of NP string is too close to the organic−metal interface, and we did not see high absorption enhancement for this position.

For a single NP string, we decreased l from 250 to 50 nm, which is equivalent to changing the string to a single NP. The enhancement in photocurrent and weighted absorption ($\langle A_w \rangle$) as a function of string length is plotted in Figure 5c. We see that, as the string length decreases, the photocurrent enhancement goes down from ∼2.1% to ∼0.3% because of the less scattering of light by the NPs. This supports the better performance of solar cells where NPs form aggregates as opposed to the cells with discrete NPs. The photocurrent enhancement exceeds that of the weighted absorption since the

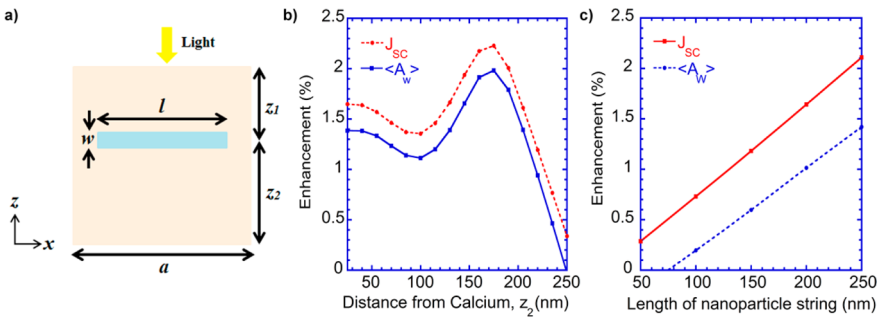

Figure 5. (a) Side view of the solar cell with single NP string at an optimum distance of $z_2 = 170$ nm. The NP string is illustrated in light blue color. The background color represents the organic layer. (b) Photocurrent and weighted absorption enhancement as a function of distance of string from calcium (z_2) electrode. (c) Photocurrent and weighted absorption enhancement as a function of length (l) of NP string.

DOI: 10.1021/acs.jpcc.5b08581
J. Phys. Chem. C 2015, 119, 23883−23889

photocurrent preferentially weighs the longer wavelengths (eq 15 in SI), where larger enhancements are found (see the EQE enhancement in Figure S6). To calculate the enhancement in photocurrent and weighted absorption, the reference flat cells have the same volume of absorber material as in the cell with NP strings.

In order to obtain a higher loading (~3 vol %), we simulate three equidistant NP strings of the same length separated by distance b in the active-layer of the solar cell (Figure 6a). For

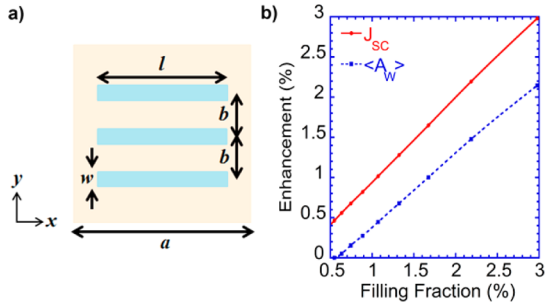

Figure 6. (a) Top view of three equidistant NP strings within the organic layer. (b) Photocurrent and weighted absorption enhancement as a function of filling fraction of the NP strings.

the simulations with multiple strings, the optimum string length is ~500 nm, which is close to the wavelength region of interest over which light scattering occurs. We varied the lattice period (a) from 600 to 1500 nm in order to obtain a loading ranging from ~3% to ~0.5%, similar to that in the experiments. The enhancement increases linearly with loading (Figure 6b). For loading ~3%, the photocurrent and weighted absorption enhancements are 3% and 2.1%, respectively. The enhancement is due to the scattering of light by the NP strings. As loading decreases, the enhancement goes down linearly as there is less scattering of light by the NPs. The scattering of light is proportional to the refractive index contrast between the dielectric and the organic, which at optical wavelengths is not very high (2.4/1.8≈1.33), thereby limiting the amount of absorption enhancement. The large dielectric constant of BTO does not play a role in absorption enhancement at optical frequencies.

To see how the NP strings behave as they form aggregates, we varied the spacing (b) between the two strings on either side of the central string for a constant lattice period of 600 nm and string length of 500 nm. When the three NP strings are touching each other (b ~ 50 nm), as shown in Figure 7a, the

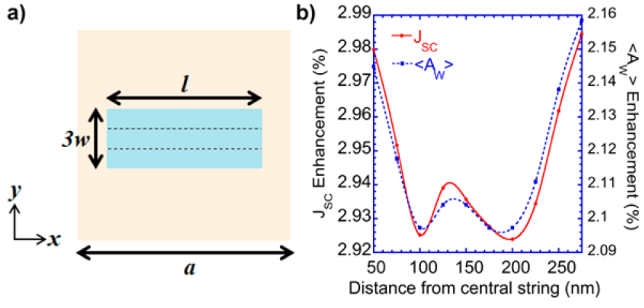

Figure 7. (a) Top view of the nanoparticle strings in the organic layer when they touch each other. (b) Photocurrent and weighted absorption enhancement as a function of separation (b) between the nanoparticle strings.

maximum J_{sc} enhancement of ~3% is obtained (Figure 7b). It is to be noted that when the distance (b) of the strings on either side of the central string reaches ~275 nm, the J_{sc} enhancement again goes to ~3%. This corresponds to the geometry when the two NP strings touch each other along the square lattice boundary to form aggregates. The larger enhancement with the NP aggregates is due to higher light scattering. There is a weak maximum in the enhancement for intermediate separation of b ~ 130 nm, which corresponds to a separation of ~340 nm of the strings in adjacent unit cells in the y-direction. This weak maximum may be due to the optical separation between the strings approaching the wavelength of red photons ($\sim \lambda/n_{org}$) inside the organic layer, which may enhance the optical scattering.

7. CONCLUSIONS

In summary, we investigated the addition of both neat and functionalized BTO particles to P3HT:PCBM based solar cells. The neat BTO particles showed mostly large aggregates, while the f-BTO particles exhibited two distinct morphologies: (1) long, string-like aggregates and (2) small agglomerates of nanoparticles. The morphologies with string-like aggregates demonstrated a 40% increase in photocurrent due to a balance of increased light scattering and optimal charge collection. The other morphology with low-level aggregation demonstrated only a slight enhancement in J_{sc} and was typically accompanied by reduced FF, which was attributed to increasing trap states with f-BTO particle additions.

Our simulation using the excitonic drift-diffusion model demonstrated that the functional group completely negates the large enhancement in exciton dissociation found with the neat nanoparticle. The increase in electric field strength, though, assists carrier transport and leads to slightly enhanced performance. Optical scattering matrix simulations demonstrate increased light scattering with string-like aggregates and enhanced photocurrents, consistent with experimental results of solar cell enhancements. For aggregated nanoparticles, both optical simulations and transmission measurements show increased light scattering that increases with the aggregate weight fraction. Even more light scattering may occur in full devices due to more roughness of the metal electrode caused by the particles. Future works could include developing techniques to disperse neat particles, discovering conducting or high dielectric constant coupling agents, or finding techniques to remove the coupling agent via postprocessing without disturbing the active-layer.

■ ASSOCIATED CONTENT

Supporting Information

The Supporting Information is available free of charge on the ACS Publications website at DOI: 10.1021/acs.jpcc.5b08581.

SEM images of active-layers deposited from a common solution containing f-BTO that was stirred for varying times. Contour plots of exciton dissociation rate, recombination rate, and electric field strength from the excitonic drift-diffusion model. Dark current−voltage, dielectric constant vs frequency, and external quantum efficiency plots. Simulation methods for both excitonic drift-diffusion model and scattering matrix method. Experimental methods for sample fabrication and characterization (PDF).

DOI: 10.1021/acs.jpcc.5b08581
J. Phys. Chem. C 2015, 119, 23883−23889

AUTHOR INFORMATION

Corresponding Author

*Tel.: 515-294-0606. E-mail: sumitc@iastate.edu.

Notes

The authors declare no competing financial interest.

ACKNOWLEDGMENTS

This material is primarily based on work supported by the National Science Foundation under Grants CBET-1236839 and ECCS-1055930. B.G. and P.D. acknowledge partial support from KAUST CRG and NSF Grant CMMI-1149365. R.B. acknowledges partial support from the Ames Laboratory, operated for the Department of Energy (theoretical analysis) by Iowa State University under Contract No. DE-AC02-07CH11385; and the National Science Foundation through Grants ECCS-1232067 and CBET-1336134 (computational work). The research used resources at the National Energy Research Scientific Computing Center (NERSC), which is supported by the Office of Science of the USDOE under Contract No. DE-AC02-05CH11231.

REFERENCES

(1) Green, M. A.; Emery, K.; Hishikawa, Y.; Warta, W.; Dunlop, E. D. Solar Cell Efficiency Tables (Version 45). *Prog. Photovoltaics* **2015**, *23*, 1−9.

(2) Kirchartz, T.; Taretto, K.; Rau, U. Efficiency Limits of Organic Bulk Heterojunction Solar Cells. *J. Phys. Chem. C* **2009**, *113*, 17958−17966.

(3) Huang, J.-S.; Goh, T.; Li, X.; Sfeir, M. Y.; Bielinski, E. A.; Tomasulo, S.; Lee, M. L.; Hazari, N.; Taylor, A. D. Polymer Bulk Heterojunction Solar Cells Employing Förster Resonance Energy Transfer. *Nat. Photonics* **2013**, *7*, 479−485.

(4) Ferenczi, T. A.; Muller, C.; Bradley, D. D.; Smith, P.; Nelson, J.; Stingelin, N. Organic Semiconductor:Insulator Polymer Ternary Blends for Photovoltaics. *Adv. Mater.* **2011**, *23*, 4093−7.

(5) Nalwa, K. S.; Carr, J. A.; Mahadevapuram, R. C.; Kodali, H. K.; Bose, S.; Chen, Y.; Petrich, J. W.; Ganapathysubramanian, B.; Chaudhary, S. Enhanced Charge Separation in Organic Photovoltaic Films Doped with Ferroelectric Dipoles. *Energy Environ. Sci.* **2012**, *5*, 7042.

(6) Yuan, Y.; Reece, T. J.; Sharma, P.; Poddar, S.; Ducharme, S.; Gruverman, A.; Yang, Y.; Huang, J. Efficiency Enhancement in Organic Solar Cells with Ferroelectric Polymers. *Nat. Mater.* **2011**, *10*, 296−302.

(7) Stratakis, E.; Kymakis, E. Nanoparticle-Based Plasmonic Organic Photovoltaic Devices. *Mater. Today* **2013**, *16*, 133−146.

(8) Topp, K.; Borchert, H.; Johnen, F.; Tunc, A. V.; Knipper, M.; von Hauff, E.; Parisi, J.; Al-Shamery, K. Impact of the Incorporation of Au Nanoparticles into Polymer/Fullerene Solar Cells. *J. Phys. Chem. A* **2010**, *114*, 3981−3989.

(9) Xue, M.; Li, L.; Tremolet de Villers, B. J.; Shen, H.; Zhu, J.; Yu, Z.; Stieg, A. Z.; Pei, Q.; Schwartz, B. J.; Wang, K. L. Charge-Carrier Dynamics in Hybrid Plasmonic Organic Solar Cells with Ag Nanoparticles. *Appl. Phys. Lett.* **2011**, *98*, 253302.

(10) Itskos, G.; Othonos, A.; Rauch, T.; Tedde, S. F.; Hayden, O.; Kovalenko, M. V.; Heiss, W.; Choulis, S. A. Optical Properties of Organic Semiconductor Blends with near-Infrared Quantum-Dot Sensitizers for Light Harvesting Applications. *Adv. Energy Mater.* **2011**, *1*, 802−812.

(11) Jarzab, D.; Szendrei, K.; Yarema, M.; Pichler, S.; Heiss, W.; Loi, M. A. Charge-Separation Dynamics in Inorganic-Organic Ternary Blends for Efficient Infrared Photodiodes. *Adv. Funct. Mater.* **2011**, *21*, 1988−1992.

(12) Nam, M.; Lee, S.; Park, J.; Kim, S.-W.; Lee, K.-K. Development of Hybrid Photovoltaic Cells by Incorporating Cuins2quantum Dots into Organic Photoactive Layers. *Jpn. J. Appl. Phys.* **2011**, *50*, 06GF02.

(13) de Freitas, J. N.; Grova, I. R.; Akcelrud, L. C.; Arici, E.; Sariciftci, N. S.; Nogueira, A. F. The Effects of CdSe Incorporation into Bulk Heterojunction Solar Cells. *J. Mater. Chem.* **2010**, *20*, 4845.

(14) Liu, Z.; Seo, S.; Lee, E.-C. Improvement of Power Conversion Efficiencies in Cr2o3-Nanoparticle-Embedded Polymer Solar Cells. *Appl. Phys. Lett.* **2013**, *103*, 133306.

(15) Lu, Y.; Alexander, C.; Xiao, Z.; Yuan, Y.; Zhang, R.; Huang, J. Utilizing Insulating Nanoparticles as the Spacer in Laminated Flexible Polymer Solar Cells for Improved Mechanical Stability. *Nanotechnology* **2012**, *23*, 344007.

(16) Lenes, M.; Kooistra, F. B.; Hummelen, J. C.; Van Severen, I.; Lutsen, L.; Vanderzande, D.; Cleij, T. J.; Blom, P. W. M. Charge Dissociation in Polymer:Fullerene Bulk Heterojunction Solar Cells with Enhanced Permittivity. *J. Appl. Phys.* **2008**, *104*, 114517.

(17) Carr, J. A.; Chaudhary, S. On Accurate Capacitance Characterization of Organic Photovoltaic Cells. *Appl. Phys. Lett.* **2012**, *100*, 213902.

(18) Walter, T.; Herberholz, R.; Müller, C.; Schock, H. W. Determination of Defect Distributions from Admittance Measurements and Application to Cu(in,Ga)Se2 Based Heterojunctions. *J. Appl. Phys.* **1996**, *80*, 4411−4420.

(19) Kodali, H. K.; Ganapathysubramanian, B. A Computational Framework to Investigate Charge Transport in Heterogeneous Organic Photovoltaic Devices. *Comput.Methods in Appl.Mech.Eng.* **2012**, *247−248*, 113−129.

(20) Kodali, H. K.; Ganapathysubramanian, B. Computer Simulation of Heterogeneous Polymer Photovoltaic Devices. *Modell. Simul. Mater. Sci. Eng.* **2012**, *20*, 035015.

(21) Kodali, H. K.; Ganapathysubramanian, B. Sensitivity Analysis of Current Generation in Organic Solar Cells—Comparing Bilayer, Sawtooth, and Bulk Heterojunction Morphologies. *Sol. Energy Mater. Sol. Cells* **2013**, *111*, 66−73.

(22) Petrovsky, V.; Petrovsky, T.; Kamlapurkar, S.; Dogan, F. Dielectric Constant of Barium Titanate Powders near Curie Temperature. *J. Am. Ceram. Soc.* **2008**, *91*, 3590−3592.

(23) Guo, X. Insulator-to-Semiconductor Transition of Nanocrystalline Batio3 at Temperatures < /=200 Degrees C. *Phys. Chem. Chem. Phys.* **2014**, *16*, 20420−3.

(24) Huang, L.; Chen, Z.; Wilson, J. D.; Banerjee, S.; Robinson, R. D.; Herman, I. P.; Laibowitz, R.; O'Brien, S. Barium Titanate Nanocrystals and Nanocrystal Thin Films: Synthesis, Ferroelectricity, and Dielectric Properties. *J. Appl. Phys.* **2006**, *100*, 034316.

(25) Lee, B.; Zhang, J. Preparation, Structure Evolution and Dielectric Properties of Batio3 Thin Films and Powders by an Aqueous Sol−Gel Process. *Thin Solid Films* **2001**, *388*, 107−113.

(26) Min, B.; Moon, S. M.; Cho, N. H. Structural and Dielectric Features of Nb-Doped Nano-Sized Batio3 Powders Prepared by Hydro-Thermal Synthesis Methods. *Curr. Appl. Phys.* **2011**, *11*, S193−S196.

(27) Sakabe, Y.; N, W.; Hamaji, Y. Grain Size Effects on Dielectric Properties and Crystal Structure of Fine-Grained Batio3 Ceramics. *J. Korean Phys. Soc.* **1998**, *32*, S260−S264.

(28) Biswas, R.; Xu, C. Nano-Crystalline Solar Cell Architecture with Absorption Beyond the Classical 4n2 Limit. *Opt. Express* **2011**, *19*, A664−A672.

(29) Li, Z.-Y.; Lin, L.-L. Photonic Band Structures Solved by a Plane-Wave-Based Transfer-Matrix Method. *Phys. Rev. E: Stat. Phys., Plasmas, Fluids, Relat. Interdiscip. Top.* **2003**, *67*.10.1103/PhysRevE.67.046607

(30) Peer, A.; Biswas, R. Nanophotonic Organic Solar Cell Architecture for Advanced Light Trapping with Dual Photonic Crystals. *ACS Photonics* **2014**, *1*, 840−847.

DOI: 10.1021/acs.jpcc.5b08581
J. Phys. Chem. C 2015, 119, 23883−23889